Biased Motion-Adaptive Temporal Filtering for Speckle Reduction in Echocardiography

Adrian N. Evans* and Mark S. Nixon

Abstract— **This paper describes a new fully motion-adaptive spatio-temporal filtering technique to reduce the speckle in ultrasound images. The advantages of this approach are demonstrated in echocardiographic boundary detection and in comparison with other techniques. The first stage of many automated echocardiographic image interpretation schemes is filtering to reduce the amount of speckle noise. We show how the two-dimensional least mean squares (TDLMS) filter can be configured as a motion-compensated filter for a time sequence of ultrasound images that eliminates the blurring associated with direct averaging. For an image corrupted by multiplicative speckle noise, the mode of the intensity distribution approximates the maximum likelihood estimator. In consequence, the temporal filter's output is biased towards the mode from the mean, using information contained within the speckle itself. A new adaptive algorithm for controlling the filter's convergence is also included. To evaluate performance, application to simulated, phantom, and an *in vivo* test sequence of the carotid artery are considered in comparison with other techniques. The effect of filtering on edges is of great importance, as these are used by subsequent image interpretation schemes. Quantitative measurements demonstrate the effectiveness of the Biased TDLMS filter, for both noise reduction and edge preservation. Echocardiographic images have a high noise content and suffer from poor contrast. Despite this challenging environment, the Biased TDLMS filter is shown to produce images that are better inputs for subsequent feature extraction. The benefits for echocardiographic images are highlighted by considering the problems of mitral valve analysis and extraction of the left atrium boundary.**

I. Introduction

ULTRASOUND (US) is a commonly used modality for cardiac imaging since it is noninvasive and real-time. However, its inherently poor image quality has consistently hampered attempts to automatically evaluate the cardiac function through spatial analysis of the left ventricular endocardial and epicardial boundaries in two-dimensional echocardiographic images. Even with the advent of transesophageal echocardiography, which improves image quality, difficulties still exist due to low spatial resolution, high speckle content, and frequently discontinuous reflections from the myocardium boundaries.

Many techniques have been proposed to automatically interpret anatomical boundaries in echocardiographic images, with the motivation being to remove the requirement for laborious manual tracing of contours which is often prone to error. Application of simple edge detection algorithms do not produce satisfactory results and must be augmented by further image interpretation. Echocardiographic boundary detection schemes generally comprise of three main stages: smoothing, contour extraction, and grouping. The first two stages attempt to produce a faithful representation of the true edge points in the image. The final step is the identification of a single, smooth contour which corresponds to the desired anatomical boundary. Han *et al.* have applied a knowledge-based approach [1] to aid these processes while Chou *et al.* [2] have used relaxation to identify the epicardial boundary. Radial searching is often used to reduce the edge detection problem from two dimensions to one [3]. Other high-level techniques that have been used for automated or semi-automated echocardiographic boundary detection include simulated annealing [4], mathematical morphology [5], fuzzy reasoning [6] and optical flow [7]; these are often computationally expensive and reflect the problem's complexity.

While much research effort has been dedicated to the edge detection and subsequent grouping tasks, smoothing the echocardiographic image to reduce speckle has received relatively little attention. This is surprising as many proposed techniques seek to use higher level knowledge to refine and augment the results of initial edge detection operators [8], [6], [4] and better initial boundaries would therefore reduce the constraints placed upon subsequent processes. Massay *et al.* [9] have applied an adaptive filter based on that of Bamber and Daft [10] to a single frame of echocardiographic data and studied the effect of reducing speckle on the definition and measurement of anatomical boundaries. To overcome the low quality of a single echocardiographic frame, compared with many noncardiac applications, speckle suppression schemes proposed for echocardiography often seek to incorporate temporal information. This contrasts with US images of other anatomical targets where advanced adaptive, single-image filters have been developed, that can accommodate the wide variation in image statistics.

Freidland and Adam included temporal information from adjacent frames in a simulated annealing method for ventricu-

Manuscript received March 13, 1995; revised October 30, 1995. This work was supported in part by a UK SERC studentship to A. N. Evans. The Associate Editor responsible for coordinating the review of this paper and recommending its publication was R. Martin. *Asterisk indicates corresponding author.*

*A. N. Evans is with the Department of Production Technology, Massey University, Palmerston North, New Zealand (e-mail: a.n.evans@massey.ac.nz).

M. S. Nixon is with the Department of Electronics and Computer Science, University of Southampton, UK.

Publisher Item Identifier S 0278-0062(96)01223-2.

lar cavity [4] and Zwehl *et al.* [11] temporally averaged three frames, weighting the central frame by two compared with the weighting for the outer frames, before applying a spatial filter. Neither method can reduce speckle with high temporal correlation since both techniques only consider a sequence of three frames. The optical flow method of Mailloux *et al.* [7] produces information of image movement over time but requires input images with a smooth spatial derivative; this is achieved by applying a 15×15 mean filter to each frame. Alternatively, Klingler *et al.* [5] average the images from a number of heart cycles and include a motion detection and rejection algorithm, though further interaction is required to confirm that the remaining frames exhibit no apparent motion.

None of the above are true three-dimensional filter structures and though they incorporate temporal information, they do so in a limited way. Simply extending an established spatial filter from two to three dimensions by including time has been found to result in the blurring of the moving edges [12]. Here we adopt the philosophy that to successfully integrate a larger number of frames into a three-dimensional filter structure, a degree of motion adaptability must be introduced. Exploiting temporal redundancy has particular application to echocardiographic imaging, where the single frame image quality is low.

The maximum likelihood (ML) estimator for an image corrupted by speckle noise with unity expected value occurs at the modal value of the intensity distribution. Unfortunately, the mode can rarely be directly obtained from a small distribution, which may be multi-modal or display a mode that does not accurately reflect the underlying distribution. This is generally the case for distributions defined by local regions of interest and instead the mode must be estimated indirectly. The truncated median filter has been used to extract the mode to reduce speckle [13] but this was restricted to restoring single frames.

To translate this concept for image sequences, we take as our starting point the two-dimensional least mean squares (TDLMS) filter of Hadhoud and Thomas [14]. This has properties which make it attractive for temporal filtering and can reduce noise while preserving moving edges. Its function is equivalent to a mean-based filter but, using statistics of the speckle noise itself, the filter's output can be adaptively modified from the mean toward the mode. Additionally we propose an adaptive technique to control the filter's convergence, to increase smoothing in homogeneous regions while retaining sharp edges at discontinuities.

The organization of this paper is as follows: Section II-A demonstrates the mode as the ML estimator for speckle noise, Section II-B shows how the TDLMS filter can be used as a spatio-temporal filter to reduce speckle in US images, Section II-C details how its performance can be improved by biasing its output toward the mode, and Section II-D describes the adaptive convergence control. In Section III the performance of the filter is established in application to simulated, phantom, and *in vivo* images of the carotid artery, in comparison with standard averaging and the original TDLMS technique. Section IV shows the advantages that this new technique can accrue in application to improving the quality of echocardiographic images. Conclusions are made in Section V.

II. Spatio-Temporal Speckle Filtering

A. Speckle Filtering

Noise suppression is a fundamental stage of many automatic contour extraction schemes for echocardiographic images. This is generally achieved by prefiltering, often with a relatively low degree of complexity. To reduce speckle in single frame US images, several advanced adaptive spatial filters have been proposed. These exhibit increased edge preservation while retaining a strong smoothing action in speckle affected regions. The adaptive Kalman filter of Castellini *et al.* [15] used image statistics to improve speckle reduction. However, the underlying Kalman filter theory assumptions, that the noise is white and Gaussian with zero mean, are not valid and the technique is restricted to one dimension; B-mode images must be filtered on a line-by-line basis. Sun and Venetsanpoulos [16] have investigated adaptive noise filtering and edge detection schemes for several noise distributions using a minimum mean square error criteria, though only additive noise was considered. Adaptive smoothing of images with signal-dependent noise using a nonstationary mean nonstationary variance model has been proposed by Kuan *et al.* [17] and subsequently applied to speckle corrupted images Kuan *et al.* [18]. This research developed a model for speckle based on the physical process of coherent image formation and used the correlation properties of speckle to further enhance the filter's performance. An alternative approach after Koo and Park [19] used image statistics to find the maximum homogeneous region surrounding each predetermined seed region and then output the arithmetic mean of the region, a strategy that was demonstrated to have good edge preserving properties.

The adaptive weighted median filter of Loupas *et al.* [20] and the unsharp masking filter of Bamber and Daft [10] (as applied to echocardiographic images by Massay *et al.* [9]) use local image statistics to vary the output between the original value and the median or mean of a local region, respectively. In both cases the ratio of the local mean to the local variance controls the output, tending toward the original image data where the ratio is low, thus improving the performance of the filter at discontinuities and providing the mean or median values in homogeneous regions. Neither the median nor the mean can be considered an optimal estimator for US images. Modeling speckle as multiplicative Rayleigh distributed noise, such that

$$z = m \times n \tag{1}$$

where m is the signal component and n is the Rayleigh distributed noise component with unity standard deviation, yields a Rayleigh distributed observed signal, z, given by

$$p(z) = \begin{cases} \frac{z}{\sigma^2} \exp\left(\frac{-z^2}{2\sigma^2}\right) & \text{if } z > 0 \\ 0 & \text{otherwise} \end{cases} \tag{2}$$

where σ^2 is the variance. Kotropoulos *et al.* [21] have shown the L_2 sealed by a constant mean to be the ML estimator of the original US B-mode image of a constant signal and more recently have shown that it provides a close approximation to the

ML estimator for the displayed US image [22]. Alternatively, the maximum of the Rayleigh distribution provides a value of the underlying signal, consistent with the ML estimator, which by differentiation occurs at

$$\frac{\partial p(z)}{\partial z} = 0 = \frac{1}{\sigma^2} \exp\left(\frac{-z^2}{2\sigma^2}\right)\left(1 - \frac{z^2}{\sigma^2}\right) \tag{3}$$

and this identifies a value for the corrupted signal of $z = \sigma$ which maximizes the probability density function; this value is the statistical mode. Displayed B-mode images are modified so that their statistical properties no longer resemble those of Rayleigh distributed noise, most noticeably by logarithmic compression. The use of the mode as an estimator has the advantage of being invariant to logarithmic compression but may be effected by other image processing functions, used by some scanners to produce the displayed B-mode image. Crawford *et al.* [23] have investigated the characteristics of ultrasound scanners, with respect to the performance of adaptive speckle reduction, and presented an inverse transform that returns the statistical properties of speckle regions to a Rayleigh distribution for those scanners that exhibit a nonlinear relationship between local variance and mean.

B. Spatio-Temporal Speckle Reduction

Although temporal redundancy is a rich source of information, few dedicated fully three-dimensional spatio-temporal filters have been proposed for US images. Many US scanners offer the option of frame averaging to reduce the speckle but this blurs moving edges. Mochizuki *et al.* [24] have used a volume based three-dimensional median/median filter, whose output is the median value of the medians from one-dimensional lines of sight through the pixel of interest in a reconstructed voxel-based image. Consideration for feature movement has to date constrained the evolution of spatial filters into the time dimension; typically only two or three frames are used.

The TDLMS filter [14] is an extension of the adaptive LMS algorithm to two dimensions and can be configured as a multi-input, single-output motion-compensated filter for image sequences. It has several properties that favor its application to US images: it does not require any signal preparation or alignment (providing the shift in feature position is within the filter window), it produces a large signal to noise ratio (SNR) improvement for low SNR inputs, and it is relatively computationally inexpensive. The operation of the filter can be explained with reference to Fig. 1 and by considering the application of the filter to a time sequence of frames. At each iteration the first frame in the sequence is used as the desired response (d_j) and the remaining frames form the reference inputs. Each reference input is convolved with its weight matrix to produce a value which is summed with those of the other reference inputs, producing the output value and, by subtraction from the desired response, the error signal. This is repeated on a pixel by pixel basis. At the next iteration the first frame is removed and replaced as the desired response by the next frame in the sequence and a new frame is added. More formally, if X_{ji} is a square $N \times N$ moving window on the

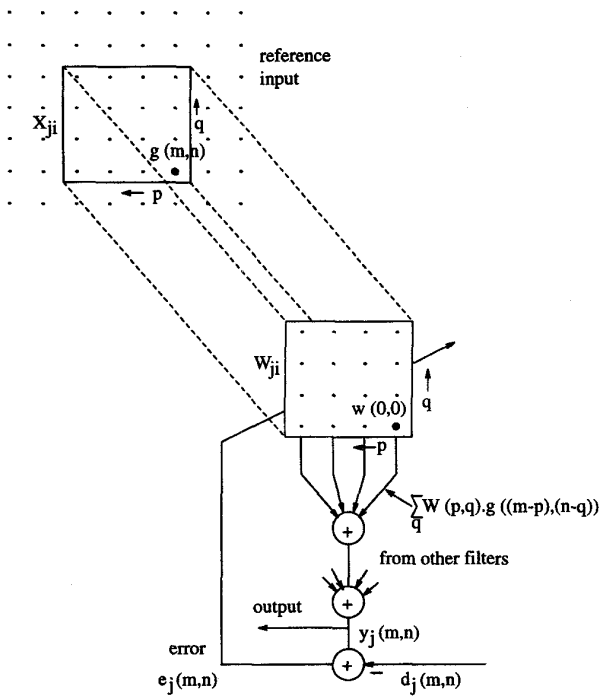

Fig. 1. Operation of the TDLMS filter.

image g_i at the i^{th} input and iteration j, then, for a sequence of k images, an input vector matrix X_j of dimensions $(k-1)N$ by N can be constructed as

$$X_j = [X_{j1} \;\; X_{j2} \;\; \cdots \;\; X_{j(k-1)}]^T \tag{4}$$

where k is the number of images. A weight vector matrix W_j of the same dimensions can be defined similarly and the output for image point, y_j, is given by the inner product

$$y_j = W_j^T \cdot X_j = X_j^T \cdot W_j. \tag{5}$$

This output y_j is the new estimate at that point in the frame $i = 0$ and the new image is the result of this window operation repeated across the entire image. The best result, y_j, that the TDLMS filter can achieve, in terms of SNR improvement, is one comparable with that of direct-averaging; the TDLMS output is equivalent to the mean of the filtered signal.

The error signal at each image point, e_j, is formed by subtracting the output response from the desired response d_j, which is the value of frame $i = 0$ for that point, giving

$$e_j = d_j - y_j = d_j - X_j^T \cdot W_j. \tag{6}$$

Using the method of steepest descent for weight updating and estimating the instantaneous gradient yields the Widrow-Hoff LMS algorithm (Widrow *et al.* [25]) which derives new weight values W_{j+1} by correcting the previous values according to error signal

$$W_{j+1} = W_j + 2Ue_jX_j \tag{7}$$

where the convergence factor U controls both the speed of convergence and the residual error.

C. Biasing the TDLMS Output

It has been shown in Section II-A that the mode, corresponding to an approximation of an ML estimator, is a good representation of the underlying image intensity for speckle corrupted US images. Determining the modal value therefore appears advantageous but unlike the mean or median values it may not be statistically accurate for small populations; consider the difficulty in deciding which of the 25 intensities contained within a 5×5 window is the modal value, when all may be different. To ascertain a close approximation to the modal value an indirect method that uses properties of the local amplitude histogram of speckle noise is proposed.

Recalling that the TDLMS filter's output corresponds to the mean, we develop this model by considering the expectations of the mean and mode for a Rayleigh distribution [26]

$$\text{Mean} = \sqrt{\frac{\pi\sigma^2}{2}} \qquad \text{Mode} = \sigma.$$

The ratio of the mean to the mode is thus given by $\sqrt{\frac{\pi}{2}}$. For pure Rayleigh statistics, this provides a method of estimating the mode, having found the mean with the TDLMS filter. However, displayed US images conform to a Rayleigh model only when the number of scattering sites within the imaging resolution cell is large, resulting in fully developed speckle. When the number of scatterers is small the probability density function is modified; with less speckle the variance of the distribution is reduced and the mode is closer to the mean. When specular reflection occurs the mean, median, and mode are congruent. The mode can therefore be approximated by the mean/$\sqrt{\pi/2}$ for fully developed speckle, by the mean for specular reflection, and by somewhere between these two extremes for partially developed speckle.

When biasing the TDLMS filter's output to an appropriate output value, a means of determining the amount of speckle present is required. A fundamental measure that is widely used to determine the local speckle content is the SNR given by the ratio of the mean to the standard deviation of those pixels contained within a local region

$$SNR = \frac{\bar{x}}{\sigma}. \tag{8}$$

For fully developed speckle, the SNR has an expected value of 1.91 [27]. As the amount of speckle decreases the SNR rises, reaching infinity for specular reflection. To gauge the degree of departure from fully developed speckle we form the SNR difference by

$$SNR_{\text{diff}} = \begin{cases} SNR - 1.91 & \text{if } SNR \geq 1.91 \\ 0 & \text{otherwise} \end{cases} \tag{9}$$

and adaptively bias the output of the TDLMS filter by

$$O_{\text{BIAS}} = \frac{O_{\text{TDLMS}}}{\sqrt{\frac{\pi}{2}}} + k \times SNR_{\text{diff}} \left(O_{\text{TDLMS}} - \frac{O_{\text{TDLMS}}}{\sqrt{\frac{\pi}{2}}} \right) \tag{10}$$

where O_{TDLMS} and O_{BIAS} are the outputs of the TDLMS filter before and after biasing toward the mode, respectively. The constant k scales SNR_{diff} to make the product $k \times SNR_{\text{diff}}$ lie between zero and unity, ensuring the output O_{BIAS} does not exceed the mean in cases of high SNR. The output O_{BIAS} for specular reflection equals O_{TDLMS} while for fully developed speckle O_{BIAS} equals $O_{\text{TDLMS}}/\sqrt{\pi/2}$, hence the mode, as required. A suitable value for k results in O_{BIAS} being slightly greater than the modal value and closer to the value of the median. This is advantageous since at edges the mode can be considered a harsh operator as the output is essentially restricted to one of the bimodal population peaks [28]. Indeed, by choosing an appropriate value of k, the TDLMS filter's output can be modified to match the characteristics required by the application. Fig. 2 shows the distributions of the outputs produced by the TDLMS and Biased TDLMS filters, with various values of k, when filtering a series of independent images of pure Rayleigh data with a mode of 30 and a mean intensity level of 37.6. Also shown is the theoretical distribution of the median of the Rayleigh distribution, obtained using order statistics theory, as presented in Appendix A. The TDLMS filter's output is centered on the known mean of the distribution, as anticipated. With $k = 0.35$ the Biased TDLMS filter mimics the operation of a median filter, with a distribution very close to that of the theoretical median, and should therefore display the well-known edge preserving and noise reduction characteristics. It should be stressed that this is the median of a three-dimensional spatio-temporal data cube, rather than simply the spatial median. When $k = 0$, the resulting population's distribution is focused on the mode and has thus elicited the ML estimator of the underlying distribution.

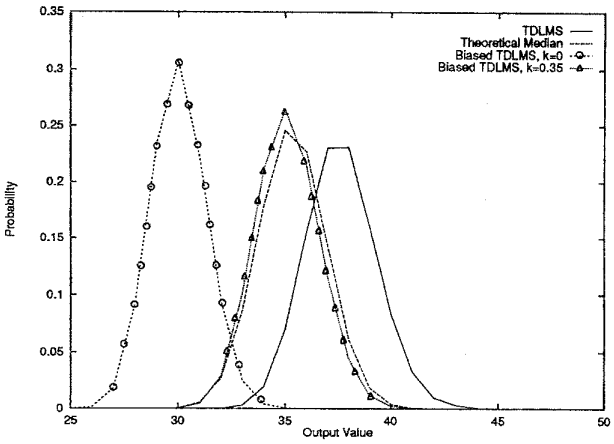

Fig. 2. Theoretical distribution of median for Rayleigh population with $\sigma = 30$; output of TOLMS and Biased TDLMS filters for simulated Rayleigh images with $\sigma = 30$.

The SNR is affected by other image components as well as speckle; for example, a feature boundary will result in a low local SNR. Biasing the output of the TDLMS filter will still occur as the SNR measure cannot identify the cause of its reduction, only the effect. In cases of low SNR, O_{BIAS} is lowered to below the mean value, and the effect at edges is to slightly reduce the output, introducing a form of edge enhancement or crispening. This is illustrated in Fig. 3 for a line of sight crossing the arterial wall in an *in vivo* scan

of the carotid artery. Fig. 3(b) shows the SNR through the artery/tissue interface and (c) displays the output of Direct Average, TDLMS and Biased TDLMS filters. It can be seen that the Biased TDLMS has produced a smooth, well localized output, with steep edge gradients and it can be anticipated that this will improve the performance of subsequent edge detection algorithms. This profile is typical of that found at edges within the image.

The potential advantages of the Biased TDLMS filter are thus two-fold: improved speckle reduction by approximating the ML estimator and clearer, stronger edges at (moving) feature boundaries.

D. Adaptive Control of Convergence

The Widrow-Hoff weight update (7) has a convergence factor U that can be optimized to produce satisfactory results. Starting with an arbitrary initial weight vector, the algorithm will converge and remain stable providing U lies between zero and the reciprocal of the largest eigenvalue, $\lambda_{\max}$, of the input autocorrelation matrix $[X_j X_j^T]$

$$0 < U < \frac{1}{\lambda_{\max}}. \tag{11}$$

This leaves many possible values for U, the choice of which will affect both the rate of convergence and the residual error.

For image processing applications, the assumption that images possess stationary spatial statistics is rarely valid. Additionally, there is a strong correlation between successive input image masks. Hadhoud and Thomas [14] have presented an analysis of the TDLMS algorithm that takes into account the nonstationarity and the correlation of input data, giving an expression for the mean square error (MSE) as

$$\text{Total } MSE = \text{Stationary } MSE + \text{Lag } MSE$$

where the Stationary MSE is the same as for the stationary inputs case and the Lag MSE is due to time variation in the inputs. For nonstationary signals, it is not necessary that the TDLMS algorithm converges to its optimum weights, but it must be able to follow variations in the signal statistics. A suitable value for the convergence factor will enable the filter to track changes in the image data over time, preserving edges, and to smooth noise in homogeneous areas. The local mean of the intensity value also influences the convergence but its effect can be minimized by ensuring the sum of the weights is set equal to unity [29], $\sum_{i=1}^{N}\sum_{j=1}^{N} W(i,j) = 1$. Though convergence is guaranteed for a wide range of initial weight values, better initial values can reduce the number of iterations required. For the implementations reported here, the initial weight values were set equal to the reciprocal of the number of image points used, simply given by the product of the mask size and the number of frames. Careful selection of initial weights is equivalent to starting the algorithm further down the learning curve.

Alexander and Ragala [30] have used a visual fidelity criteria to derive an optimal value for the convergence factor. An important conclusion from their work and that of Hadhoud and Thomas [14] is that satisfactory results can be produced by using a value for the convergence factor that only approximates the optimal value and they further demonstrated that a wide variation in image statistics does not produce extreme variations in the optimum value for the convergence factor; acceptable results can be produced for the TDLMS filter for an order of magnitude variation in the convergence factor. For specific applications trial and error can be used to find a

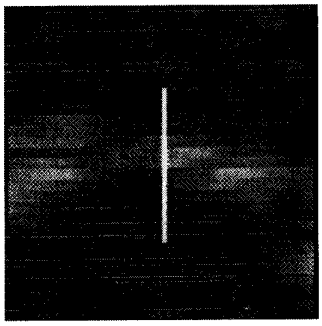

(a)

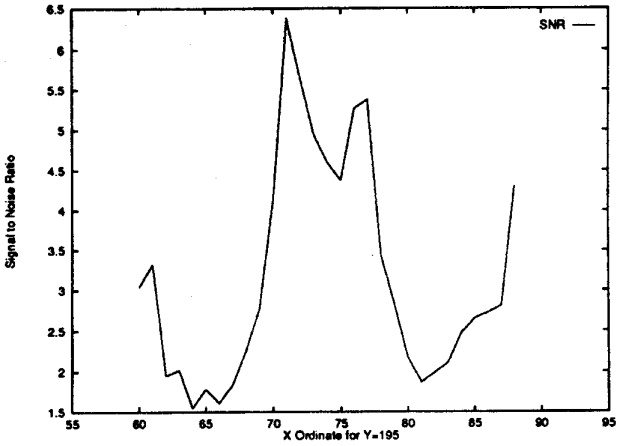

(b)

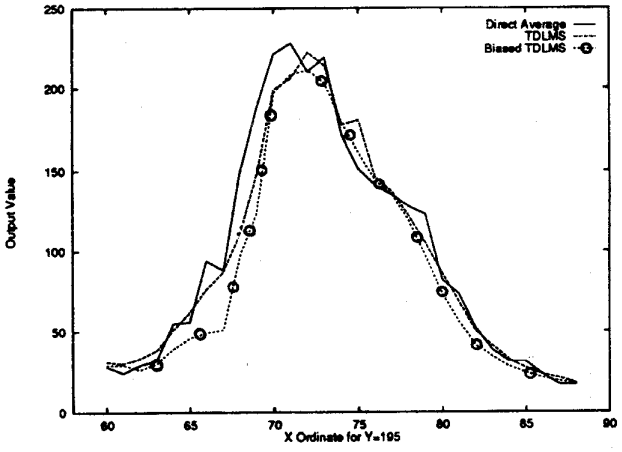

(c)

Fig. 3. Effect of Biased TDLMS filter at edges (a) cross section through arterial wall, (b) SNR along cross section and (c) output of direct averaging, TDLMS and Biased TDLMS filters.

suitable value of U. Alternatively, self-optimization methods do not require an *a priori* knowledge of the image statistics and are invariant to image sequences.

Harris *et al.* [31] have proposed a variable step (VS) algorithm that uses the gradient of the error surface to increase or decrease the current value of U within a specified range of $U_{\min}$ to $U_{\max}$. The method of individual parameter adaptation, proposed by Mikhael *et al.* [32], used signal dependent constants to individually adapt filter parameters, using a matrix of convergence factors. Individual matrix elements adapt the filter parameters that promise a larger reduction of the error signal to a greater extent than those parameters offering a lesser reduction, improving performance in nonstationary images.

None of these techniques obtain directly for speckle corrupted US images; here we describe a signal-adaptive technique for convergence control that is used throughout this paper. For US images, a convergence factor must be chosen that can follow any movement present to preserve features of interest that are moving in time. However, when there are no feature boundaries present, this requirement is redundant, and instead it is desirable to smooth the speckle corrupted region. In practice, images consist of regions containing feature boundaries and uniform areas, and it therefore appears sensible to choose a convergence factor U that is higher at feature boundaries, to follow motion and preserve edges, and lower in continuous regions to provide more smoothing. By adapting U locally, the spatial variance of images can be compensated for and a better result should ensue. The success of adaptive methods in single image US filters argues well for such an approach.

The question of how to adapt U to local image statistics needs to be addressed. One measure that has been used to characterize image regions locally is the SNR which is high in uniform regions and low at discontinuities, precisely the response that can be used to adaptively adjust U. As the Biased TDLMS filter involves the local SNR at each image point, no additional computational cost is incurred. The range of values for U in which the filter will operate satisfactorily is finite and defined by the upper and lower bounds, $U_{\max}$ and $U_{\min}$, of [31]. The local SNR is calculated (8) at each point, using the values within a moving window centered on that point from each frame in the time sequence to calculate the mean and standard deviation values. Including this in the weight update equation produces an adaptive weight update equation

$$W_{j+1} = W_j + \frac{c \times U}{SNR^2} e_j X_j \tag{12}$$

where c is the constant of adaptivity such that $U_{\min} \leq \frac{c \times U}{SNR^2} \leq U_{\max}$. The affect of the SNR is controlled by the power of the denominator; the square of the SNR produces a suitable variation of the effective convergence factor within the predefined range.

E. Summary of New Technique

The conventional implementation of the TDLMS technique is contained in (4), (5) and (6), producing output y_j. Weight updating is then carried out in accordance with (7). The Biased TDLMS filter uses this value for y_j in (10) ($O_{\text{TDLMS}} = y_j$) to provide the new estimate, O_{BIAS}, at each point. Equation (12) is used for adaptive weight updating, using the original value of y_j to ensure convergence to the mean value.

III. Experimental Results

Within the framework of automatic image interpretation, the filtering operation aims to improve the suitability of the image for subsequent processes. The effect of filtering on the position and contrast of the edges within the image is of critical importance as it is this information that often provides the basis for further analysis. Application of an edge detector, being analogous to primary feature extraction, provides a means of assessment. Our aims are therefore different from many existing schemes for evaluating speckle reduction, since these are usually concerned with the observable diagnostic value of the resulting image. Application to simulated, phantom, and *in vivo* sequences is used to establish the performance to the Biased TDLMS filter in comparison with the standard TDLMS filter and direct averaging. By using a simulated image, the probability of speckle affecting an image point and the position of edges can be tightly controlled but this is fundamentally restricted as we are interested in what happens to real edges in US images. The approach adopted here additionally uses a circular plastic pipe in a water bath to provide a real B-scan image, with all the limitations of the imaging system, containing an object of known dimensions, allowing objective measurements of the filters' performance on edges. The final test sequence is an *in vivo* scan of the carotid artery. A single image from each test sequence is shown in Fig. 4, the *in vivo* image has undergone logarithmic compression, as it is this form that is familiar to radiologists.

Measures that have been proposed to determine the amount of speckle present within an image include the contrast to speckle ratio (CSR) of Patterson and Foster [33], introduced as an attempt to quantify the ability of an observer to perceive anechoic areas against a background of speckle. It measures the image contrast of cylindrical voids in a random scattering medium relative to the contrast fluctuation due to speckle and is given by

$$\text{CSR} = \frac{\bar{x}_o - \bar{x}_i}{(\sigma_o^2 + \sigma_i^2)^{1/2}} \tag{13}$$

where $\bar{x}_i$ and σ_i^2, respectively, are the average signal value and the variance inside the void and $\bar{x}_o$ and σ_o^2 are those outside the region. In addition to the CSR, local SNR measures (8) can be used to measure the speckle reduction at discrete locations in an image. In an homogeneous region the SNR measures the amount of speckle whereas at a discontinuity the local SNR indicates the degree of edge preservation, little SNR improvement over that of the original, unfiltered image being synonymous with no modification.

The results presented in the following sections used a kernel size of 5×5. For single frame adaptive filters, the kernel size relates to the size of the observed speckle cell. With spatio-temporal filtering, the kernel is three dimensional and must be large enough in spatial dimension to contain the interframe

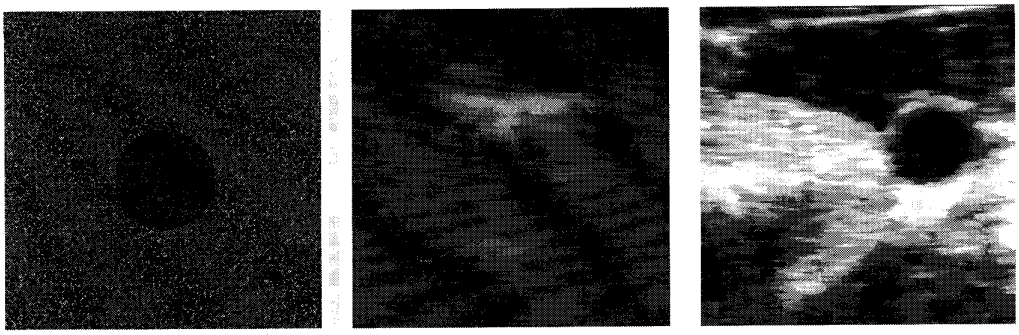

(a) (b) (c)

Fig. 4. Single images from test sequences (a) simulated, (b) phantom and (c) *in vivo*.

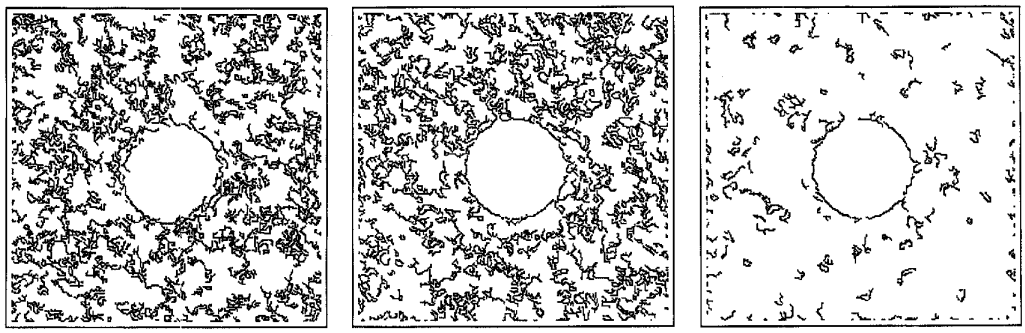

(a) (b) (c)

Fig. 5. Edge detected simulated test sequence results: (a) direct averaging, (b) TDLMS, and (c) Biased TDLMS.

movement of features. All local SNR and CSR measurements were taken using a 5 × 5 mask, matching the filter size.

A. Simulated Test Sequence

The simulated test sequence consisted of a series of eight 256 × 256 images of fully developed speckle containing a central circular region of lower underlying intensity than the background. In each frame the coordinates of this circle were varied, producing motion from the upper left to lower right of the image. The center coordinates for successive frames were (128, 128), (130, 128), (130, 130), (132, 130), (132, 132), (134, 132), (134, 134), and (136, 134), where ($x = 0$, $y = 0$) corresponded to the top left corner of the image. These coordinates were chosen to isolate any artifacts introduced by horizontal and vertical movement. To imitate a continuous sequence these frames were recycled; at each iteration one frame provides the desired response and the remainder formed the reference inputs that were adaptively filtered.

The results produced by direct averaging, TDLMS, and Biased filters for the simulated test sequence, after Canny edge detection [34], are shown in Fig. 5. Application of an edge detection stage allows observations on the influence of filtering on edges to be assessed. In each case the threshold was adjusted to produce the best result in terms of removing spurious edge responses while preserving the feature boundary, thus highlighting the relative strength of the true and false edge points. Two aspects of these results are of particular interest: speckle reduction and performance at edges. Inspection of Fig. 5 reveals that the number of edge responses due to speckle noise is similar for direct averaging and TDLMS filtering and dramatically reduced by the Biased TDLMS filter; this is confirmed by the total number of edge points found for each image which are 12 357, 12 056, and 2929, respectively. Local SNR measurements are 5.31 for direct averaging, 5.98 for TDLMS and 8.68 for Biased TDLMS, with each value being the average of the reading from 10 localities. For comparison the SNR of an original single frame was 1.91, the expected value for a Rayleigh distribution. As no anechoic regions exist in these simulated images, the CSR is not an appropriate measure.

The edge response to the circular disc can be divided into two categories. In the lower left and upper right quadrants of the disc the edges are regions where the edges present are parallel to the direction of motion of the disc; here the response is well defined and reasonably continuous, though the effect of direct averaging has been to elongate and straighten the edges. The upper left and lower right quadrants display edges are normal to the direction of motion. Fig. 5(a) has broken, insubstantial edges and also shows a multiple response to the single edge present, caused by severe blurring. In contrast the motion adaptive methods [Fig. 5(b) and(c)] show a clearer, more continuous response.

B. Phantom Test Sequence

To obtain the phantom image sequence a section of hard circular plastic pipe was moved slowly in a water bath, while the transducer was held in a fixed position by a clamp, producing a series of images with interframe motion approximately

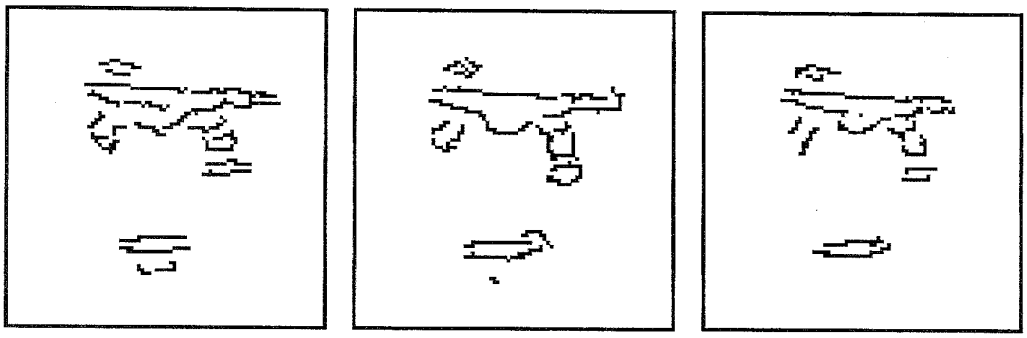

(a) (b) (c)

Fig. 6. Edge detected phantom test sequence results: (a) direct averaging, (b) TDLMS, and (c) Biased TDLMS.

ranging between two and four pixels; the direction of motion roughly followed an arc moving left and upwards. Mixing fine particles of chalk with the water surrounding the phantom introduced various degrees of partially developed speckle, with the amount being dependent on the distribution of the chalk particles. Eight frames from the time sequence were used for direct averaging and to provide the ideal and reference inputs for the motion-adaptive techniques at each iteration.

Using the response of the Canny edge detector on the phantom sequence of images, the strength and positional accuracy of the edges present can be evaluated. Evidence of blurring is present in the right side of Fig. 6(a) where smearing has resulted in longer, straighter edges that do not correspond with the known structure of the phantom, but instead are a result of the motion. Here, the inner and outer edges of the phantom that are normal to the direction of motion have not been well detected and at the bottom of the phantom the edges are slightly elongated. This situation is ameliorated by the TDLMS and Biased TDLMS filters.

We are interested in the number of edge points found that are congruent with the known physical position of the edge points, characterized by two concentric circles. By considering the ratio of the number of edge points that match the ideal edge to the total number of edge points a quantitative measure can be obtained, row two of Table I. Also given is the improvement upon the result from an original, unfiltered, single frame. However, this measure is very precise and gives no credit to those techniques which produce points that are close to, but not exactly on, the ideal edge points. Accommodating this, a match is said to occur if an edge point coincides with any of the eight nearest neighbors of the ideal edge points, giving row three of Table I. Row one of Table I gives the actual number of edge points found; a reduction in this number accompanied by an increase in the match ratios is analogous to the removal of false edge points while retaining the true ones. The TDLMS filter has found slightly fewer points than direct averaging but of these a higher proportion correspond with the ideal points. Better results for both exact and nearest neighbor matches have been produced by the Biased TDLMS filter.

TABLE I
RATIO OF NUMBER OF EDGE POINTS MATCHING IDEAL EDGE TO TOTAL NUMBER OF EDGE POINTS FOR PHANTOM TEST OBJECT

Filter Type	Direct Average	TDLMS	Biased TDLMS
Number of Edge Points Found	318	302	258
Exact Match (%)	13.2	14.6	18.6
Improvement on Single Frame (dB)	3.33	4.18	6.30
Nearest Neighbour (%)	43.1	44.4	46.9
Improvement on Single Frame (dB)	2.80	3.05	3.53

C. In Vivo Test Sequence

A sequence of *in vivo* scans of the carotid artery complete the test set. In the *in vivo* scans motion is introduced by two sources. First from movement of features within the image, in this case due to pulsating blood flow and second, during the scanning process the hand-held transducer moves relative to the target, either interactively to obtain a more suitable image or due to unavoidable movements, such as that produced by respiration in echocardiographic imaging. Fig. 7 displays the resultant images produced by direct averaging, TDLMS and Biased TDLMS filters; consistent with previous results eight frames of image data have been used. For interpretation, we again consider the speckle reduction and edge preservation qualities. SNR and CSR measurements in Table II gives measures for the images in Fig. 7. The SNR was taken in 10 regions of interest considered to consist predominantly of speckle and the readings averaged. For the CSR the interior of the artery was used for the anechoic region and the average of ten readings used to provide each of the values used in (13). All techniques improve upon the original image, this is apparent in the darker regions of Fig. 7 which exhibit reduced speckle. Table II quantifies the degree of improvement, for which the ranking order is: Biased TDLMS technique (greatest); standard TDLMS; direct averaging (smallest).

Although no ideal edge model exists, comparison of the Canny edge detected *in vivo* images, Fig. 8, provides a means of assessing the filters' performance. A smooth, continuous edge response at the arterial wall bears testimony to the

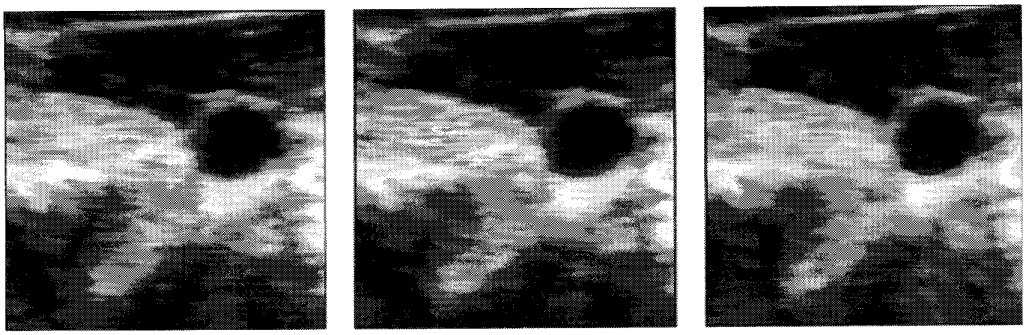

(a) (b) (c)

Fig. 7. *In vivo* test sequence results: (a) direct averaging (b) TDLMS, and (c) Biased TDLMS.

TABLE II
MEAN SNR (SD) AND CSR MEASUREMENTS FROM 10 SPATIAL LOCATIONS WITHIN *IN VIVO* IMAGES

Filter Type	Direct Average	TDLMS	Biased TDLMS
Mean SNR in Artery (σ)	13.19 (3.8)	19.26 (8.8)	20.26 (8.3)
Improvement on Single Frame (dB)	5.87	9.15	9.59
Mean SNR in Speckle (σ)	7.83 (2.6)	12.49 (6.8)	12.85 (6.7)
Improvement on Single Frame (dB)	4.69	8.75	9.00
CSR	4.80	6.34	6.58
Improvement on Single Frame (dB)	4.93	7.40	7.67

quality of the filter. The response of the Biased TDLMS filter displays a well-defined arterial wall with less residual clutter than standard TDLMS filter while direct averaging has been unable to resolve the associated movement, producing a broken, discontinuous response.

D. Results Summary

The advantages of the Biased TDLMS filter potentially offers are two-fold. Firstly the speckle reduction performance of the filter is enhanced slightly above that of the standard TDLMS filter for both the simulated and *in vivo* test sequences. Both temporal methods compare favorably in this respect with direct averaging, the improvement in the standard TDLMS filter resulting from the adaptive convergence control. The other area of importance is the influence of filtering on the edge points within the image. For the simulated image the motion-adaptive ability of the temporal filters is demonstrated and an objective assessment provided by the phantom test sequence. Biased TDLMS filtering has been shown to quantitatively produce the best results on feature boundaries, marking true boundaries with good locational accuracy and without the blurring associated with direct averaging. The smooth, continuous boundaries exhibited by the edge detected filtered images of the carotid artery confirm this point. Though these results would be strengthened by a full series of more exhaustive tests, they clearly indicate the potential advantages that the Biased TDLMS filters confers to ultrasound images

IV. APPLICATION TO ECHOCARDIOGRAPHY

Automatic interpretation of echocardiographic images is consistently limited by the low image quality. To demonstrate the advantages of the Biased TDLMS filter we consider the problem of mitral valve analysis and detection of the left atrium boundary. We do not aim to produce an optimum scheme but instead, by determining the benefits filtering confers to a standard edge detector, to establish the image improvement that is produced for any latter feature extraction stage.

Fig. 9(a) is a parasternal long axis view of the left atrium and mitral valve in early diastole, shown in the familiar logarithmically compressed form. The valve leaflets are hard to discern against the background and identification of the hinge points is difficult. Biased TDLMS filtering has produced the result in Fig. 9(c); although this image still exhibits low contrast it provides a much better input for the Canny edge detector as reflected in Fig. 9(f). Although speckle has been much reduced in the Biased TDLMS result the border of the mitral leaflets has not been dimensionally compromised and is clearer than that of the original image. For comparison the results produced by direct averaging are given in Fig. 9(b) and (e). Direct averaging has been unable to accommodate the feature movement and as a result multiple responses to a single edge abound. Further, although the clarity of the valve leaflets has been improved, because of the blurring there is little confidence on the dimensional accuracy of the feature boundaries.

A feature extraction technique for labeling the left atrium wall is applied to the original and filtered images, to illustrate the improvements afforded by the Biased TDLMS filter. For this technique the left atrium is recorded during systole and the Canny edge detector applied. Then a radial search from the atrium's center is undertaken; the first Canny edge response found is marked as wall data. There are many possible extensions to this scheme, such as using anatomical knowledge to limit the search area, but the aim here is to show the benefits of the filtering for even a simple feature extraction scheme.

The results of feature extraction are shown in Fig. 10. The original image, Fig. 10(a), highlights many of the problems

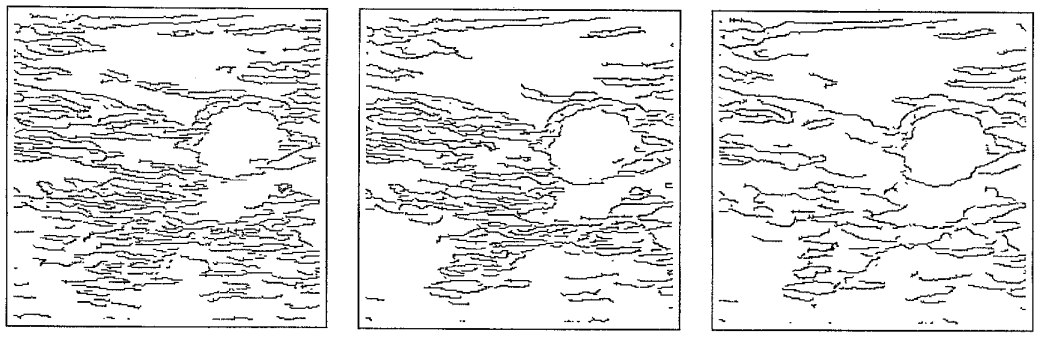

(a) (b) (c)

Fig. 8. Edge detected *In Vivo* Test Sequence results: (a) Direct averaging, (b) TDLMS; and (c) Biased TDLMS.

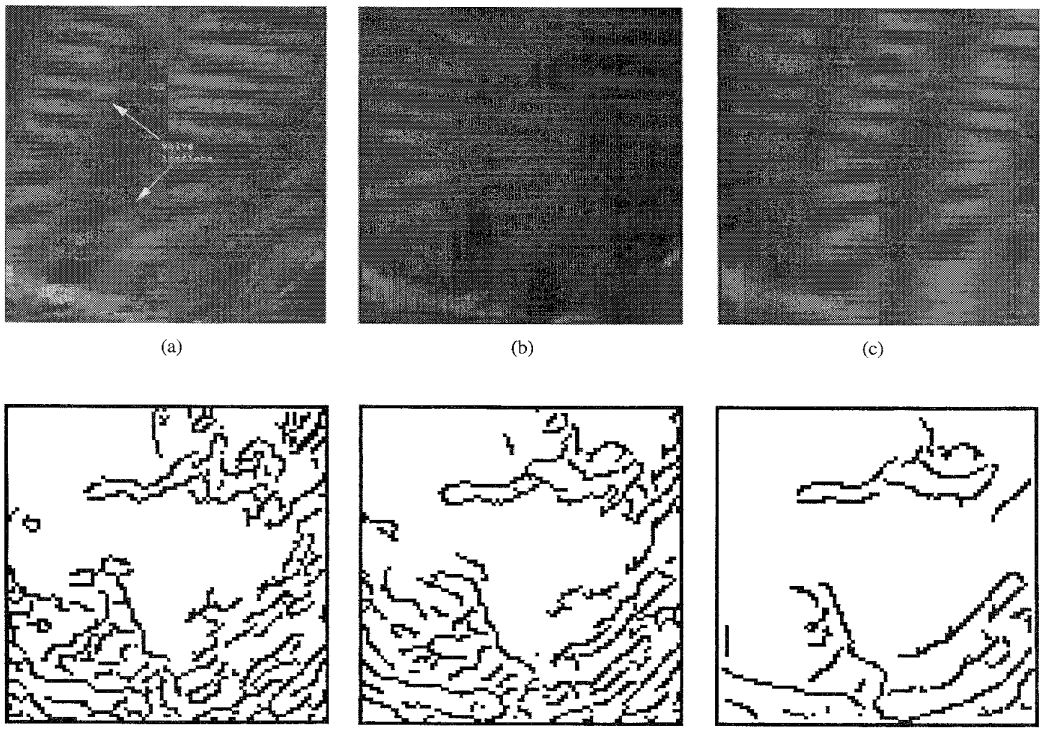

(a) (b) (c)

(d) (e) (f)

Fig. 9. Mitral value results: (a) original, (b) direct averaging, (c) Biased TDLMS, (d) edge-detected original, (e) edge-detected direct averaging; and (f) edge detected Biased TDLMS.

associated with this application; speckle is present in the center of the atrium and the atrium boundary is very fragmented giving a very poor result. Direct averaging [Fig. 10(b)] has removed some of the spurious edge points from inside the atrium and response at the atrium wall is more continuous but still unsatisfactory. The feature extraction result from the Biased TDLMS image, Fig. 10(c), shows an easily discernible improvement, devoid of speckle in the atrium and with smooth, well-connected edges at the atrium wall. Deviation from the boundary occurs mainly occurs as a result of missing edge data, a problem easily addressed by a more sophisticated technique, such as an active contour model.

This paper does not attempt to provide a clinical evaluation of the new filter in comparison with other extant techniques, both manual and automatic, for determining anatomical boundaries and subsequent measurements. The advantages that may result from using the Biased TDLMS filter in echocardiography have been shown and a full clinical appraisal is the subject of further research.

V. Conclusion

A new technique for reducing the speckle of US images has been proposed that, by incorporating temporal information, has particular application to echocardiographic imaging where the quality of a single frame is low. Motion-adaptability has been used to improve upon extant techniques by enabling a greater amount of temporal information to be included

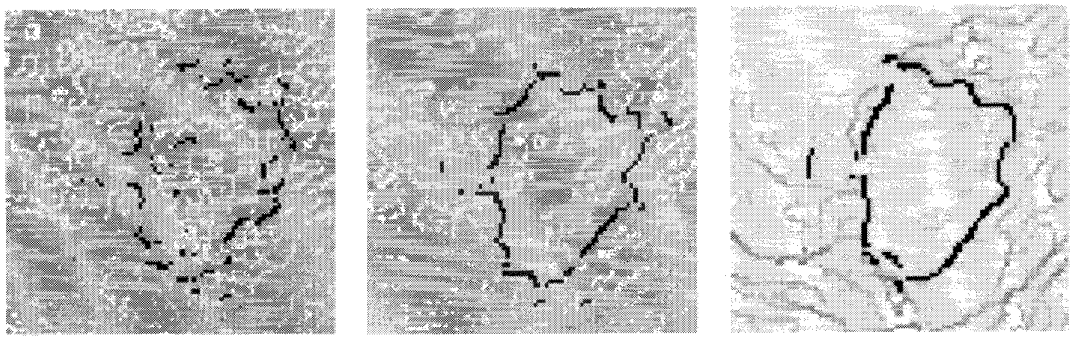

(a) (b) (c)

Fig. 10. Feature extraction stage applied to mitral valve images: (a) Original; (b) Direct average; and (c) Biased TDLMS

within the filter structure without compromising the clarity of feature boundaries. Other novel features of the filter are the use of an adaptive convergence factor and the biasing of the filter's output toward the ML estimator for speckle noise. A comprehensive results assessment shows the Biased TDLMS filter to successfully reduce speckle while preserving the anatomical boundaries of the original image. This assessment shows a better result on simulated, phantom and *in vivo* image sequences. Application of the Biased TDLMS filter to echocardiographic images has demonstrated that despite the low image contrast the results produced have high potential for use as inputs for a further automated interpretation stage. The application of a simple feature extraction technique reinforces this point. Several areas of further work have been identified. The first of these is a clinical comparison with other adaptive speckle reduction methods, to fully establish the diagnostic value of the Biased TDLMS filter in echocardiography. Integration of the filter with a computer vision method of detecting left ventricular endocardial and epicardial boundaries would provide a means of fully assessing the benefits that the Biased TDLMS filter confers to echocardiography.

Appendix A
Distribution of Median for Rayleigh Population

The theory of order statistics provides the necessary underlying theory and is used here to produce a probability density function (*pdf*) for the median of a population that is Rayleigh distributed.

If $X_1, X_2, \cdots, X_n$ are n independent variates, each with cumulative distribution function (*cdf*) $P(x)$, then the *cdf* of the rth largest order statistic $X_{(r)}$ can be given by $F_r(x)$ $(r = 1, 2, \cdots, n)$ such that

$$F_r(x) = Pr\{X_{(r)} \leq x\} = \sum_{i=r}^{n} \binom{n}{i} P^i(x)[1 - P(x)]^{n-i}.$$

Given the *pdf* of $X_i$as $p(x) = P^{'}(x)$, the *pdf* of $X_{(r)}$, denoted by $f_r(x)$, can be given by [22, ch. 2] as

$$f_r(x) = \frac{1}{B(r, n-r+1)} P^{r-1}(x)[1 - P(x)]^{n-r} p(x)$$

where $B(x, y)$ is the Euler Beta function expressed in terms of the Gamma function as

$$B(x, y) = \frac{\Gamma(x)\Gamma(y)}{\Gamma(x+y)}.$$

Thus, simplifying

$$\frac{1}{B(r, n-r+1)} = \frac{n!}{(r-1)!1!(n-r)!}.$$

The median value occurs when $r = (n+1)/2$ and therefore

$$f_{\text{med}}(x) = \frac{n!}{(\frac{n-1}{2})!(\frac{n-1}{2})!} P^{r-1}(x)[1 - P(x)]^{n-r} p(x).$$

All is that is now required is to substitute for $p(x)$ and $P(x)$ the *cdf* and *pdf* of a Rayleigh population given by

$$p(x) = \frac{x}{\sigma^2} \exp\left(\frac{-x^2}{2\sigma^2}\right) \text{ and } P(x) = 1 - \exp\left(\frac{-x^2}{2\sigma^2}\right)$$

and thus the distribution of the median for a Rayleigh population is

$$\begin{aligned} f_{\text{med}}(x) =& \frac{n!}{[(\frac{n-1}{2})!]^2}[1 - \exp(\frac{-x^2}{2\sigma^2})]^{(n-1)/2} \\ & [\exp(\frac{-x^2}{2\sigma^2})]^{(n-1)/2} \frac{x}{\sigma^2} \exp(\frac{-x^2}{2\sigma^2}) \\ =& \frac{n!}{[(\frac{n-1}{2})!]^2} \frac{x}{\sigma^2}[1 - \exp(\frac{-x^2}{2\sigma^2})]^{(n-1)/2} \\ & [\exp(\frac{-x^2}{2\sigma^2})]^{(n+1)/2}. \end{aligned}$$

Acknowledgment

The authors wish to thank Dr. T. K. Hames for his advice and comment.

References

[1] C. Y. Han, K. W. Lin, W. G. Wee, R. M. Mintz, and D. T. Porembka, "Knowledge-based image analysis for automated boundary extraction of transesophageal echocardiographic left-ventricular images," *IEEE Trans. Med. Imag.*, vol. 10, no. 4, pp. 602–610, 1991.

[2] W.-S. Chou, C.-M. Wu, and K.-H. Hsieh, "Detecting myocardial boundaries of the left ventricle from a single-frame 2-DE image," *Pattern Recog.*, vol. 23, no. 7, pp. 799–806, 1990.

[3] D. Adam, O. Hareuveni, and S. Sideman, "Semiautomated border tracking of cine echocardiographic ventricular images," *IEEE Trans. Med. Imag.*, vol. 6, no. 3, pp. 266–271, 1987.

[4] N. Friedland and D. Adam, "Automatic ventricular cavity boundary detection from sequential ultrasound images using simulated annealing," *IEEE Trans. Med. Imag.*, vol. 8, no. 4, pp. 344–353, 1989.
[5] J. W. Klingler, C. L. Vaughan, T. D. Fraker, and L. T. Andrews, "Segmentation of echocardiographic images using mathematical morphology," *IEEE Trans. Biomed. Eng.*, vol. 35, no. 11, pp. 925–934, 1988.
[6] J. Feng, W.-C. Lin, and C.-T. Chen, "Epicardial boundary detection using fuzzy reasoning," *IEEE Trans. Med. Imag.*, vol. 10, no. 2, pp. 187–199, 1991.
[7] G. E. Mailloux, M. Bertrand, and R. F. Stampfler, "Local histogram information content of ultrasound B-mode echographic texture," *Ultrasound in Med. Biol.*, vol. 11, no. 5, pp. 743–750, 1985.
[8] C. H. Chu, E. J. Delp, and A. J. Buda, "Detecting left ventricular endocardial and epicardial boundaries by digital two-dimensional echocardiography," *IEEE Trans. Med. Imag.*, vol. 7, no. 2, pp. 81–90, 1988.
[9] R. J. Massay, R. B. Logan-Sinclair, J. C. Bamber, and D. G. Gibson, "Quantitative effects of speckle reduction on cross sectional echocardiographic images," *Brit. Heart J.*, vol. 62, 1989.
[10] J. C. Bamber and C. Daft, "Adaptive filtering for reduction of speckle in ultrasonic pulse-echo images," *Ultrason.*, vol. 24, no. 1, pp. 41–44, 1986.
[11] W. Zwehl, R. Levy, E. Garcia, R. V. Haendchen, W. Childs, S. R. Corday, S. Meerbaum, and E. Corday, "Validation of a computerized edge detection algorithm for quantitative two-dimensional echocardiography," *Circ.*, vol. 68, no. 5, pp. 1127–1135, 1983.
[12] A. Schistad and T. Taxt, "Speckle reduction in ultrasound images using temporal and spatial context," in *IEEE Nucl. Sci. Symp. Med. Imag. Conf.*, 1991, pp. 2210–2214.
[13] A. N. Evans and M. S. Nixon, "Mode filtering to reduce ultrasound speckle for feature extraction," in *Proc. IEE-Vision, Image Signal Processing*, vol. 142, no. 2, pp. 87–94, 1995.
[14] M. M. Hadhoud and D. W. Thomas, "The two-dimensional adaptive LMS (TDLMS) algorithm," *IEEE Trans. Circuits Syst.*, vol. 35, no. 5, pp. 485–494, 1988.
[15] G. Castellini, D. Lamate, L. Mascotti, E. Monnini, and S. Rocchi, "An adaptive Kalman filter for speckle reduction in ultrasound images," *J. Nucl. Med. Allied Sci.*, vol. 32, no. 3, pp. 208–213, 1988.
[16] X. Z. Sun and A. N. Venetsanopoulos, "Adaptive schemes for noise filtering and edge detection by use of local statistics," *IEEE Trans. Circuits Syst.*, vol. 35, no. 1, pp. 57–69, 1988.
[17] D. T. Kuan, A. A. Sawchuk, T. C. Strand, and P. Chavel, "Adaptive noise smoothing filter for images with signal-dependent noise," *IEEE Trans. Pattern Anal. and Machine Intell.*, vol. 7, no. 2, pp. 165–177, 1985.
[18] D. T. Kuan, A. A. Sawchuk, T. C. Strand, and P. Chavel, "Adaptive restoration of images with speckle," *IEEE Trans. Acoust., Speech, Signal Processing*, vol. 35, no. 3, pp. 373–383, 1987.
[19] J. I. Koo and S. B. Park, "Speckled reduction with edge preservation in medical ultrasonic images using a homogeneous region growing mean filter (HRGMF)," *Ultrason. Imag.*, vol. 13, no. 3, pp. 211–237, 1991.
[20] T. Loupas, W. N. McDicken, and P. L. Allan, "An adaptive weighted median filter for speckle suppression in medical ultrasound images," *IEEE Trans. Circuits Syst.*, vol. 36, no. 1, pp. 129–135, 1989.
[21] C. Kotropoulos and I. Pitas, "Optimum nonlinear signal detection and estimation in the presence of ultrasonic speckle," *Ultrason. Imag.*, vol. 14, no. 3, pp. 249–275, 1992.
[22] C. Kotropoulos, X. Magnisalis, I. Pitas, and M. G. Strintzis, "Nonlinear ultrasonic image processing based on signal-adaptive filters and self-organizing neural networks," *IEEE Trans. Image Processing*, vol. 3, no. 1, pp. 65–77, 1994.
[23] D. C. Crawford, D. S. Bell, and J. C. Bamber, "Compensation for the signal processing characteristics of ultrasound B-mode scanners in adaptive speckle reduction," *Ultrasound Med. Biol.*, vol. 19, no. 6, pp. 469–485, 1993.
[24] T. Mochizuki, M. Ito, and K. Tachikawa, "Ultrasonic image processing using a three-dimensional median filter," in *Jpn. J. Appl. Phys—Proc. 11th Symp. Ultrason. Electron.*, 1991, vol. 30 s1, pp. 228–230.
[25] B. Widrow, J. R. Glover, J. M. McCool, J. Kaunitz, C. S. Williams, R. H. Hearn, J. R. Zeidler, E. Dong, and R. C. Goodlin, "Adaptive noise canceling: Principles and applications," *Proc. IEEE*, vol. 63, no. 12, pp. 1692–1719, 1975.
[26] P. Peebles, *Probability, Random Variables, and Random Signal Principles*, 2nd ed. New York: McGraw-Hill, 1987.
[27] R. F. Wagner, S. W. Smith, J. M. Sandrik, and H. Lopez, "Statistics of speckle in ultrasound B-scans," *IEEE Trans. Sonics Ultrason.*, vol. 30, no. 3, pp. 156–163, 1983.
[28] E. R. Davies, "On the noise suppression and image enhancement characteristics of the median, truncated median and mode filters," *Pattern Recog. Lett.*, vol. 7, no. 2, pp. 87–97, 1988.
[29] M. M. Hadhoud and D. W. Thomas, "The effect of the image local mean on the two-dimensional least mean square algorithm weight convergence," *J. Mod. Opt.*, vol. 36, no. 4, pp. 545–549, 1989.
[30] S. T. Alexander and S. A. Rajala, "Optimal gain derivation for the LMS algorithm using a visual fidelity criterion," *IEEE Trans. Acoust., Speech, Signal Processing*, vol. 32, no. 2, pp. 434–437, 1984.
[31] R. W. Harris and D. M. Chabries, "A variable step (VS) adaptive filter algorithm," *IEEE Trans. Acoust., Speech, Signal Processing*, vol. 34, no. 2, pp. 309–316, 1986.
[32] W. B. Mikhael, F. H. Wu, L. G. Kazovsky, G. S. Kang, and L. J. Fransen, "Adaptive filters with individual adaptation of parameters," *IEEE Trans. Circuits Syst.*, vol. 33, no. 7, pp. 677–686, 1986.
[33] M. S. Patterson and F. S. Foster, "The improvement and quantitative assessment of B-mode images produced by array/cone hybrid," *Ultrason. Imag.*, vol. 5, pp. 195–213, 1983.
[34] J. F. Canny, "A computational approach to edge detection," *IEEE Trans. Pattern Anal. Machine Intell.*, vol. 8, no. 6, pp. 679–698, 1986.